Journal of
Nuclear Engineering

MDPI

Communication

Investigation of Electromagnetic Sub-Modeling Procedure for the Breeding Blanket System

Ivan Alessio Maione [1,*], Massimo Roccella [2] and Flavio Lucca [2]

[1] Institute for Neutron Physics and Reactor Technology, Karlsruhe Institute of Technology (KIT), Hermann-von-Helmholtz-Platz 1, 76344 Eggenstein-Leopoldshafen, Germany
[2] LT Calcoli srl, Via Bergamo 60, 23807 Merate, LC, Italy
* Correspondence: ivan.maione@kit.edu

Abstract: The outcome of the electromagnetic (EM) analyses carried out during the DEMO pre-conceptual phase demonstrated that EM loads are relevant for the structural assessment of the breeding blanket (BB) and, in particular, for the definition of the boundary conditions at the attachment system with the vacuum vessel. However, within the scope of the previous campaign, the results obtained using simplified models only give a rough estimation of the EM loads inside the BB structure. This kind of data has been considered suitable for a preliminary assessment of the BB segments, but it is not considered representative as input for structural analysis in which a detailed BB internal structure (that considers cooling channels, thin plates, etc.) is analyzed. Indeed, mesh dimensions and computational time usually limit EM models that simulate a whole DEMO sector. In many cases, these constraints lead to a strong homogenization of the BB structure, not allowing the calculation of the EM loads on the internal structure with high precision. To overcome such limitations, an EM sub-modeling procedure was investigated using ANSYS EMAG. The sub-modeling feasibility is studied using the rigid boundary condition method. This method consists of running a global "coarse" mesh, including all the conducting structures that can have some impact on the component under investigation and inputting the obtained results on the detailed sub-model of the structure of interest as time-varying boundary conditions. The procedure was tested on the BB internal structure, taking as reference a DEMO 2017 baseline sector and the helium cooled pebble bed (HCPB) concept with its complex internal structure made by pins. The obtained results show that the method is also reliable in the presence of non-linear magnetic behaviour. The methodology is proposed for application in future BB system assessments.

Keywords: electromagnetism; fusion; plasma disruption; DEMO; breeding blanket

Citation: Maione, I.A.; Roccella, M.; Lucca, F. Investigation of Electromagnetic Sub-Modeling Procedure for the Breeding Blanket System. *J. Nucl. Eng.* **2023**, *4*, 165–176. https://doi.org/10.3390/jne4010013

Academic Editors: Stjepko Fazinić, Tonči Tadić and Ivančica Bogdanović Radović

Received: 31 October 2022
Revised: 19 January 2023
Accepted: 26 January 2023
Published: 30 January 2023

1. Introduction

In modern engineering, the finite element (FE) technique [1,2] is increasingly used to exploit the feasibility of very large and complex structures. Tokamaks, such as ITER [3] now under construction and DEMO [4], the proposed next DEMO-nstration fusion power plant, are typical examples of such very large and complex structures involving extremely hard technological issues in mechanical, thermo-fluid dynamic, neutronic, and electromagnetic fields. Due to this fact, these projects need an enormous amount of computer-aided engineering. This engineering work often requires the optimization of single small parts or sub-components of the whole structure. Design optimization can uniquely be achieved by iterating and repeating a slightly modified FE model to identify the best design parameters of the components by analyzing their structural performance in a given situation. As, in EM analyses, the load conditions at the component boundaries are greatly influenced by the presence of the whole structure, each iteration analysis would require a part of the structure, or the whole structure itself, to be included in the FE model, implying a complete remodeling of the whole structure at each iteration. Furthermore, the mesh refinement of

the sub-model needed to achieve the required accuracy in the numerical solutions would incur very high, often prohibitive, costs both in terms of modeling and computing time. To overcome such limitations, the sub-modeling approach [5,6] is often used as it allows more accurate results to be obtained in a particular region of the FE model by transferring the boundary conditions from a primary (coarse) to a secondary (refined) mesh. The main sub-modeling routines can be summarized into two major steps as represented in the flowchart in Figure 1.

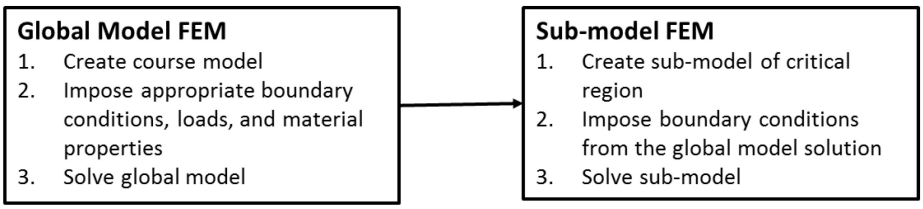

Figure 1. Basic flowchart for the FEM sub-modeling procedure.

This strategy has been applied in different engineering fields, including structural mechanics, electromagnetics, thermos-fluid dynamics, and so on [7–19]. In particular, when dealing with commercial tools, such as ANSYS EMAG, sub-modeling has mainly been used in the presence of finite elements with a magnetic nodal formulation (i.e., SOLID97) for which a DOF mapping to the boundary of the sub-model is feasible, as performed in [9,10].

The aim of this study is to analyze the possibility of extending the sub-modeling procedure to the ANSYS EM elements S236/S237 that are based on an edge-flux formulation and are much more efficient than those based on the nodal formulation in the non-linear analyses (such as those required for DEMO plant which make extensive use of ferromagnetic material, e.g., EUROFER97 [20]).

The sub-modeling feasibility is studied by applying the rigid boundary condition method. This method consists of running a global "coarse" mesh, including all the conducting structures that can have some impact on the component under investigation and inputting the obtained results on the detailed sub-model of the structure of interest as time-varying boundary conditions. The procedure was tested on the breeding blanket segment structure, taking as reference a DEMO2017 [21] toroidal sector of 22.5 degrees, the HCPB concept with its complex internal structure made by pins [22] (see Figure 2), and a fast upper plasma vertical displacement event (UVDE) with a current quench (CQ) time of 74 ms carried out with CarMa0NL [23].

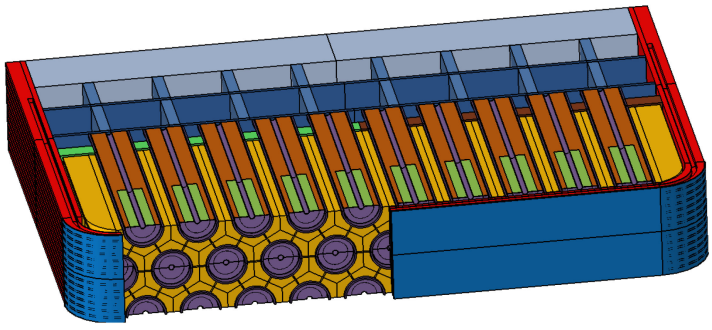

Figure 2. Example of a slice of the HCPB concept with a pin internal structure. Refer to [22] for a complete description.

Four different models, described in detail in Section 2, were implemented:

1. GDM1: global DEMO model of the whole sector with a coarse mesh used to extract the boundary conditions for the sub-model;
2. GDM2: as GDM1 but with the detailed mesh integrated into it;

3. SUB1: sub-model created using the detailed mesh and a "reasonable" element layer of the coarse mesh of GDM2;
4. SUB2: like SUB1 but using an extended section of the coarse mesh (that also includes some excitations).

The reliability test of the sub-modeling procedure was carried out as follows:

a) The transient non-linear EM analysis of the sub-model was performed, assuming as time-dependent loading conditions at its boundary nodes the DOF values obtained at these nodes from the EM analysis under the same EM transient of GDM1, which does not contain the detailed region;
b) The results obtained in the detailed region in the sub-model analysis were compared with the results obtained in the same region using the model, including the DEMO sector and the detailed region itself;
c) A comparison between the results obtained with the two sub-models was made to investigate the possibility of extending the procedure by also applying internal excitations and to reduce the error due to sub-model perturbation of the boundary conditions.

A schematic representation of the implemented FEM models and the sub-modeling procedure check is shown in Figure 3.

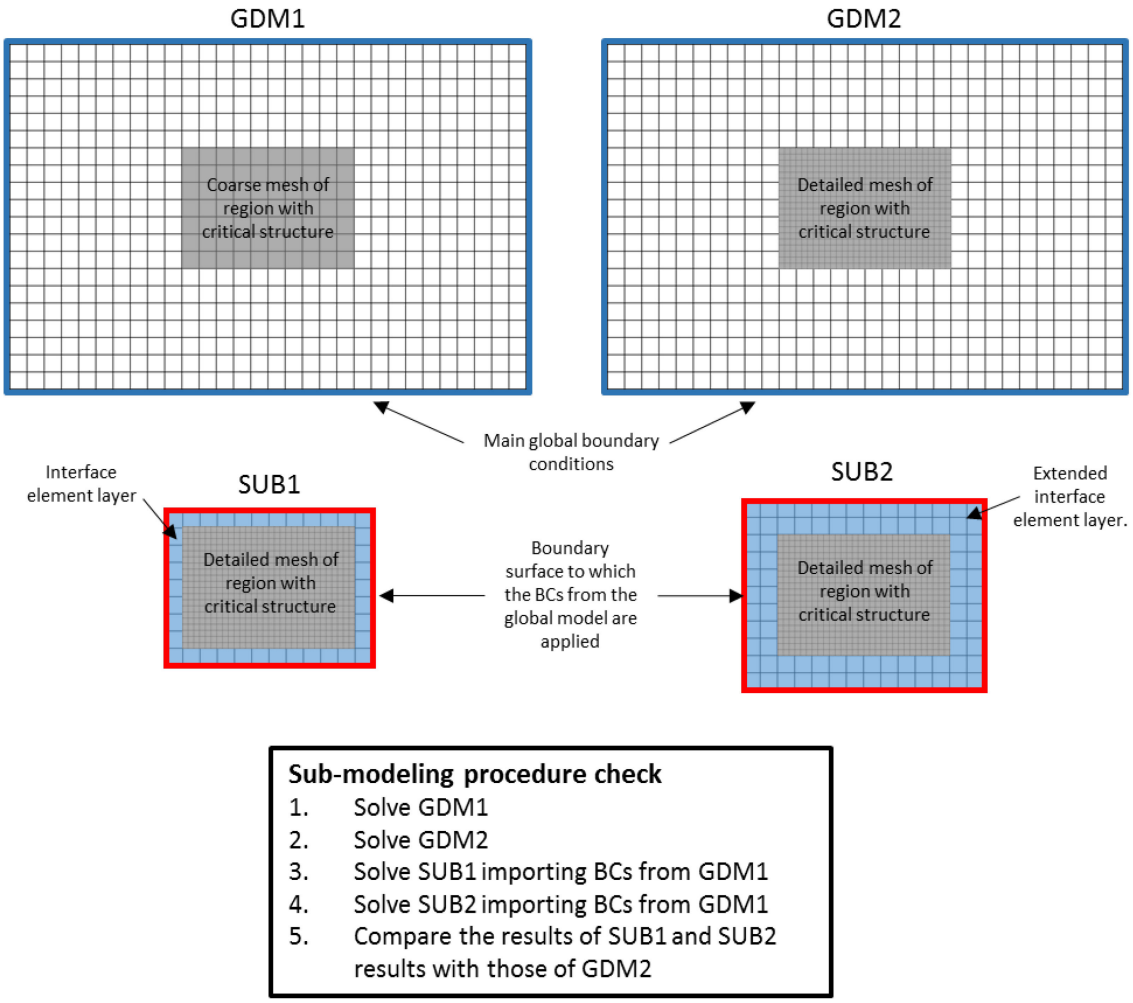

Figure 3. Schematic representation of the implemented FEM models and computational steps used to check the sub-modeling procedure.

2. Model Descriptions

As previously introduced, the study was conducted using two DEMO global models: the first one, GDM1, was modeled with enough accuracy to allow quite good precision in the evaluation of the EM loads of large components, such as the vessel, divertors, and blanket segments. In particular, the vessel, upper and equatorial ports, upper and equatorial port plugs, and the main components of the back supporting structure (BSS) of all blanket segments (the back plate, side walls, toroidal and poloidal ribs, and manifold) were modeled with a good degree of accuracy, while the first wall (FW) and the breeding zone (BZ), whose complete detail would have required an extremely high number of elements, were modeled using homogenized structures as made, for example, in [24]. A view of all the conductive structures and BB segments is shown in Figures 4 and 5, respectively.

The second global model, GDM2, is identical to the first one for most of the mesh, but a segment of about 1.3 m height of the FW and the BZ, located in the equatorial region of the central outboard blanket, was remeshed to best reproduce, inside this limited region, the real geometric characteristics of the inner sub-components of the FW and BZ (cooling channels and pins) that had been roughly considered in the first model. The two sub-models (SUB1 and SUB2) were extracted from this global model (see Figures 6 and 7).

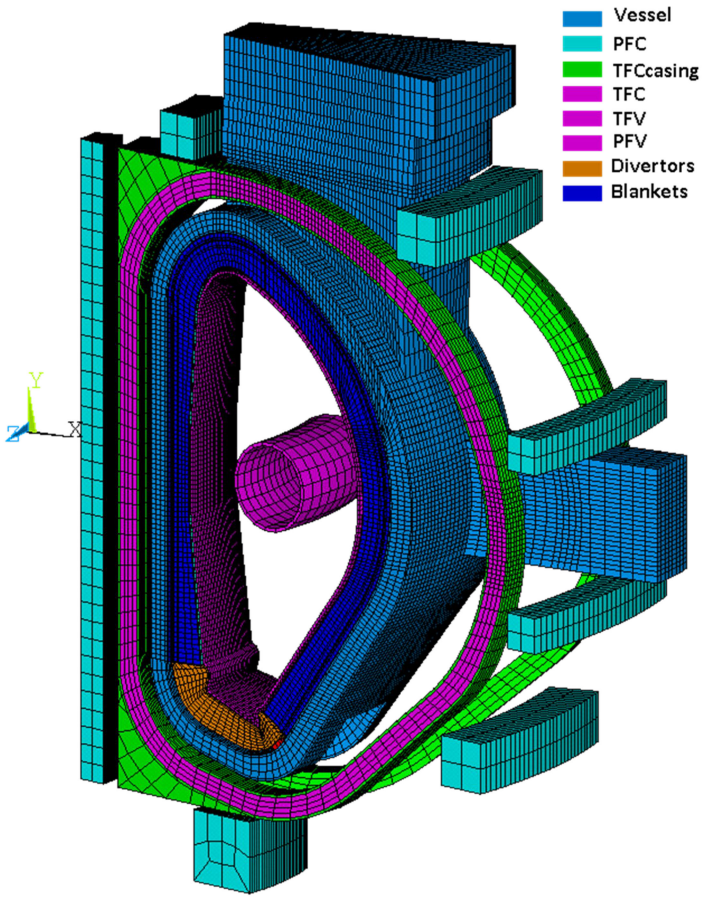

Figure 4. View of the conductive structure of the global DEMO model (GDM1). The complete electromagnetic model consists of an additional enclosure of 120 m.

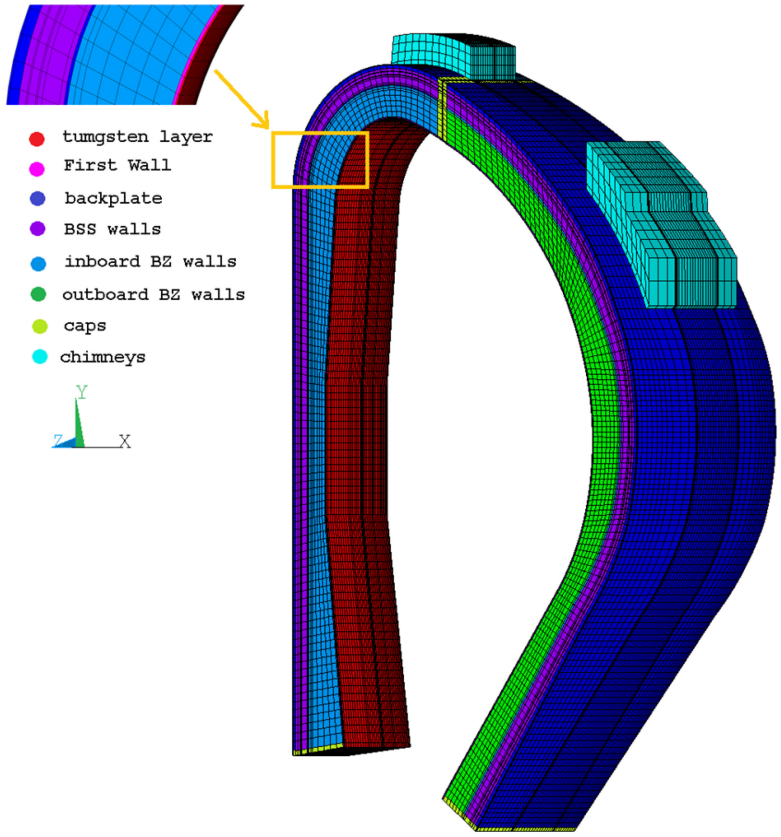

Figure 5. The five blanket segments (two at inboard and three at outboard) included in the modeled 22.5 degrees HCPB DEMO sector.

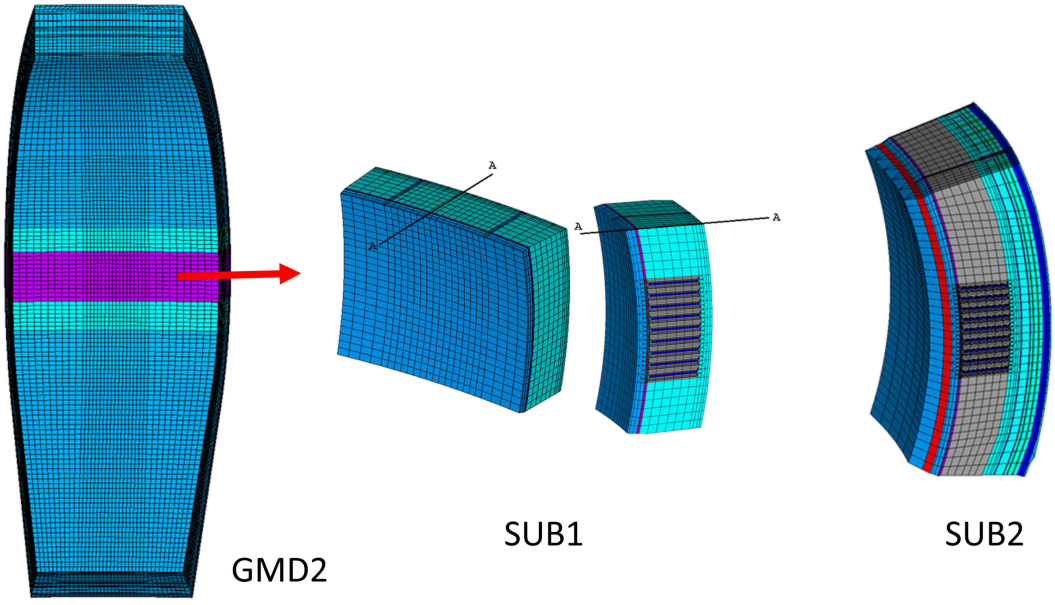

Figure 6. Details of the additional models used for the V&V of the sub-modeling procedure. The purple and light blue regions in GMD2 identify the regions from which SUB1 and SUB2 are, respectively, extracted.

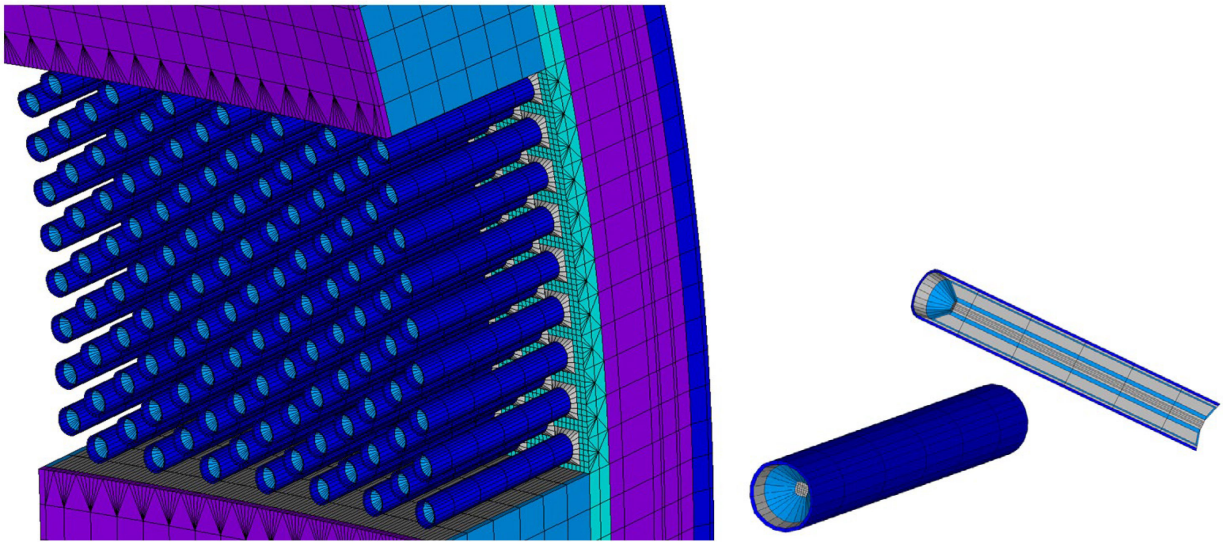

Figure 7. (Left) Mesh of the pins inside the BZ of the detailed section of the central blanket. The external wall of the detailed section of FW was hidden to show the modeling of the tight cooling channeling inside; (right) model of a single pipe pair inside the detailed section of the BZ. In grey: insulating gaps between the two nested pipes; in blue and light blue: the conducting walls of the pipes.

2.1. Element Type and Boundary Conditions

All models were developed using the ANSYS element S236, which is a 3-D 20-node element that has static and transient, linear and non-linear, EM modeling capability [25]. The element has magnetic and electric degrees of freedom (DOF). Magnetic degrees of freedom are based on the edge-flux formulation. The edge-flux (AZ) degree of freedom is defined as the line integral of the magnetic vector potential on the considered edge from the lower corner node number to the higher corner node number. It is defined at the mid-side nodes only (i.e., there are no magnetic degrees of freedom associated with the corner nodes). The analysis is driven by the current density applied as an element body load. The models use two element types: type 1 for non-conducting and type 2 for conducting materials (see Table 1 for a list of the used key options).

Table 1. Element type options used for the generation of the electromagnetic FEM models (refer to [25] for a detailed description of the used key options).

ET, 1, SOLID236	ET, 2, SOLID236	Comment
KEYOPT,1,1,0	KEYOPT,2,1,1	Magnetic and electric DOFs: (ET 1) only AZ; (ET 2) AZ, VOLT
KEYOPT,1,2,0	KEYOPT,2,2,0	Strong (matrix) coupling between magnetic and electric DOFs
KEYOPT,1,5,0	KEYOPT,2,5,0	Eddy currents effects
KEYOPT,1,7,1	KEYOPT,2,7,1	Electromagnetic force output at element corner nodes only
KEYOPT,1,8,0	KEYOPT,2,8,0	Maxwell stress tensor electromagnetic force calculation

The following boundary conditions were applied to the global models:

– Each isolated conducting component was electrically grounded fixing the VOLT DOF on one node to zero;

- Cyclic boundary conditions for the VOLT DOF are imposed using the APDL command CPCYC on the master and slave sections (toroidal boundary nodes at −11.25 and +11.25 degrees, respectively) for conducting components that cross the cyclic boundary;
- A flux parallel boundary condition (AZ = 0) is applied on the nodes of the spherical boundary surface (at a radius of 120 m) and on the axial line, with the exception of one mid-side node of the axial line near the outer surface, in order to avoid the constrain of the toroidal flux to zero;
- Coupling of AZ on the master and slave was performed with an ad-hoc APDL macro that imposes equality constraint equations (CE) taking into account the edge integral direction. This requires an equivalent mesh on the master and slave section, which was respected during the creation of GDM1 and GDM2.

2.2. Excitation Loads

The plasma disruption event, taken as a reference for this work, is a fast UVDE with a thermal quench (TQ) characteristic time of 4 ms and a current quench characteristic time of 74 ms. Plasma evolution was calculated using the CarMa0NL code, as reported in [23]. The time behaviour of the main plasma characteristics is shown in Figure 8.

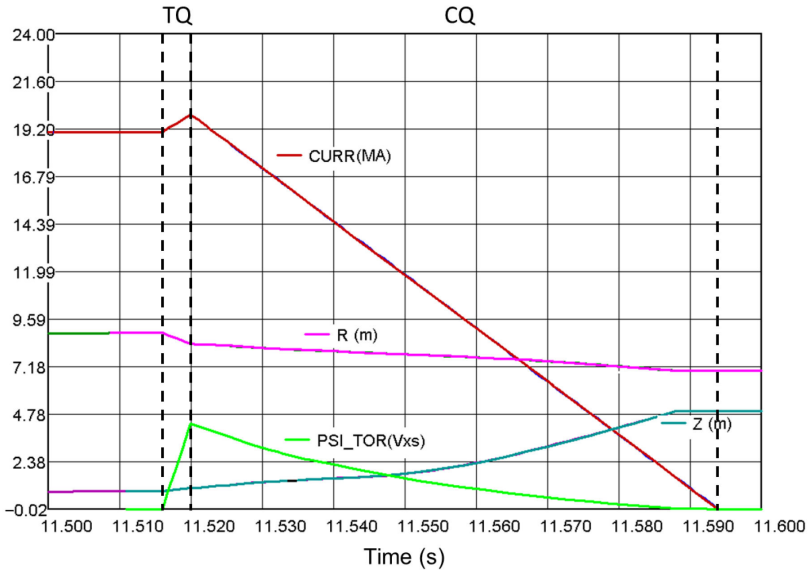

Figure 8. Time behaviour of plasma current (CURR), plasma current centroid position (in cylindrical coordinates R and Z), and plasma toroidal flux (PSI_TOR) during the considered UVDE.

The plasma behaviour was implemented through a set of toroidal filaments (PFV) with equivalent currents that simulate the poloidal magnetic field generated by the plasma outside the plasma region; and a toroidal solenoid (TFV) in the central region of the plasma for the generation of the plasma toroidal flux.

The electric currents in the toroidal field coils (TFCs), as well as in the central solenoid (CS) and the poloidal field coils (PFCs), are assumed to be constant during the plasma disruption. The current in the TFC is chosen to produce a toroidal field of 4.9T at the nominal plasma radius of 8.9. The current direction is such that both the plasma and toroidal magnetic fields are clockwise (see Figure 9).

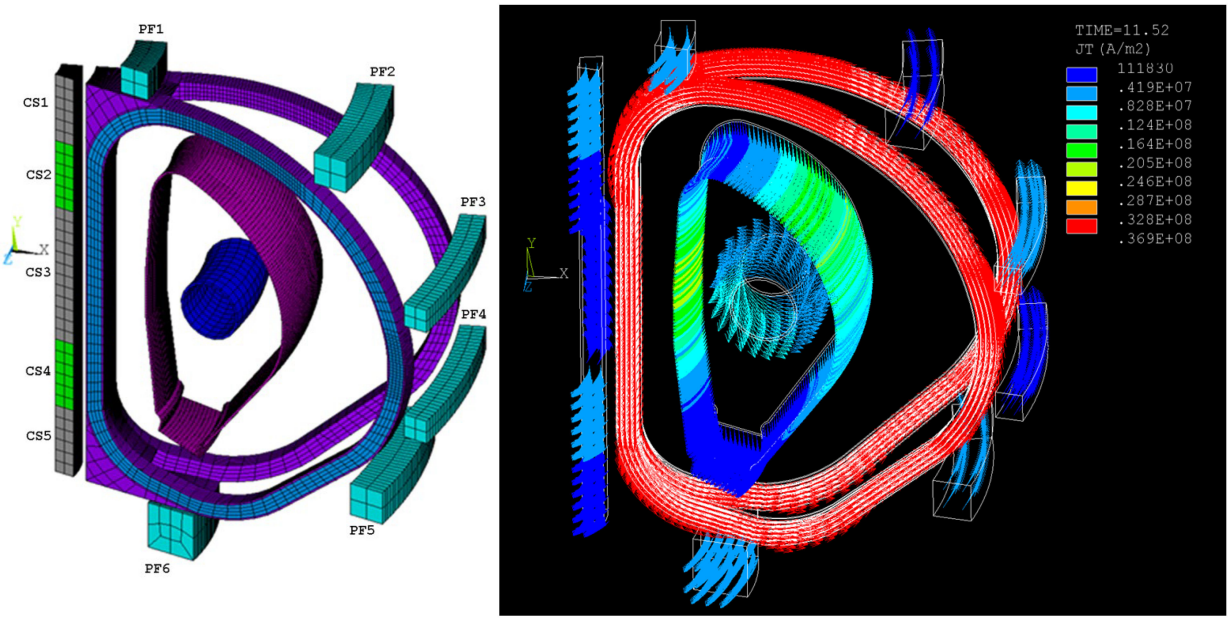

Figure 9. (Left) The EM model of the excitations used to reproduce the complete EM transient due to plasma disruption. TFC winding pack (blue-cyan), TFC casing (violet), CS (green and grey), PFCs (cyan), PFV (magenta), TFV (blue). In the modeled DEMO sector are included only two halves of one TFC at the sector boundary. (Right) Current density vector plot in the CS, PFCs, TFCs, and PFV and TFV load excitation arrays at TQ peak time.

3. Validation and Verification

The verification of the sub-modeling procedure is mainly aimed to check the correct importing of the boundary conditions into the sub-model and the feasibility of the edge-elements using time-dependent boundary conditions. It was conducted using SUB1 and GDM2 (from which the boundary conditions for SUB1 were extracted). In particular, the procedure consists of the following steps: (1) a run of GDM2 under the EM transient produced by the UVDE; (2) the extraction of the DOF values at the SUB1 boundary nodes at each time step; (3) the importing of the obtained values as boundary loads to run SUB1; (4) a comparison of the magnetic flux density (B) and current density (J) calculated running GDM2 and SUB1 in the SUB1 region at each time step. The agreement of both B and J was verified within an error lower than 0.1%. An example of the current density and magnetic field distribution inside the FW and BZ pins calculated with GDM2 at the end of the CQ is shown in Figure 10. Maximum and minimum values are also reported there. Due to the high agreement between the GDM2 and SUB1 results, the J and B plots obtained with SUB1 are omitted.

As the real goal of the sub-modeling is to perform detailed analyses of small regions without the need to run the highly time-consuming analyses of a whole model, a second step was performed. In this case, SUB1 was run assuming the DOF values at its boundary nodes as those evaluated by the same analysis performed with the GDM1 model. The obtained results were then compared with the results of the analyses performed with GDM2, and a first estimate of the reliability and precision of the used sub-modeling approach was performed. Moreover, the possibility of improving the precision of the sub-modeling procedure by extending the sub-model in such a way as to reduce the perturbation of the detailed region at the sub-model boundary was verified by performing the previous analysis using SUB2.

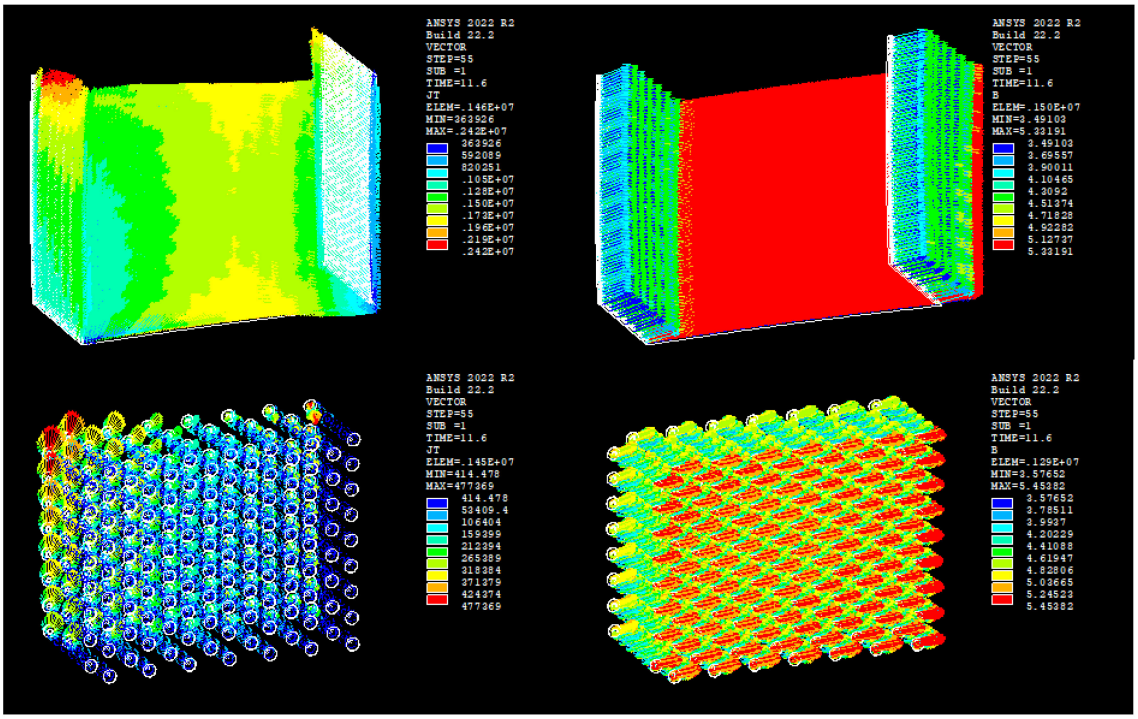

Figure 10. Example of J (left) and B (right) distribution inside the FW (top) and the BZ pins (bottom) during the EM transient calculated using GDM2 at the end of the CQ (11.6 s).

To have an estimate of the reliability of the method, the percentage deviations of the results calculated with SUB1 and SUB2 from the results obtained with the full EM model GDM2 were calculated. As a preliminary assessment, the comparison was made using the maximum values of magnetic flux density B and eddy current density J for the FW and the inner and outer pipes within the BZ calculated at the end of the thermal quench (t = 11.52 s) and at the end of the current quench (t = 11.6 s). The percentage deviation was estimated using the following equation:

$$\delta V_{subx}^{cmp} = 100 \times \left| \frac{V_{max}^{cmp}(subx) - V_{max}^{cmp}(GDM2)}{V_{max}^{cmp}(GDM2)} \right|, \quad (1)$$

where V stays for the B or J magnitude; *cmp* for one of the following components: FW, the inner or outer pipe assemblies; *subx* for the analyses of SUB1 or SUB2. The results are reported in Table 2.

Table 2. Percentage deviations of B and J calculated using Equation (1) for SUB1 and SUB2 in respect to the GDM2 reference value.

	From SUB1 Analysis (%)	From SUB2 Analysis (%)	GMD2 Reference Value
δB_{max} (FW at t = 11.52 s)	0.3	0.07	5.43 T
δB_{max} (FW at t = 11.6 s)	0.4	0.1	5.33 T
δJ_{max} (FW at t = 11.52 s)	3.0	0.9	10.2 MA/m^2
δJ_{max} (FW at t = 11.6 s)	9.0	0.8	2.42 MA/m^2
δB_{max} (Pin at t = 11.52 s)	2.2	0.7	5.69 T
δB_{max} (Pin at t = 11.6 s)	15	0.04	5.45 T
δJ_{max} (Pin at t = 11.52 s)	2.5	0.7	1.26 MA/m^2
δJ_{max} (Pin at t = 11.6 s)	5.7	0.6	0.47 MA/m^2

Furthermore, the good agreement of B and J is also reflected in the EM loads, as can be seen in Figure 11, which shows the total EM loads for the most loaded BZ pin calculated with SUB1, SUB2, and GDM2.

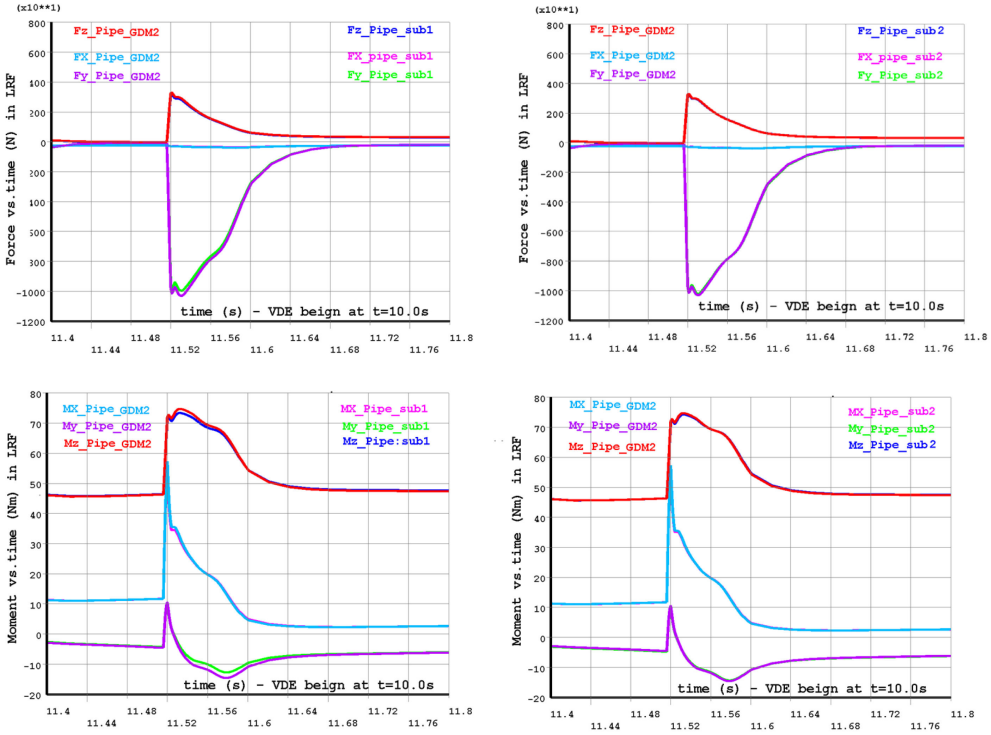

Figure 11. Components of the total EM force (Fx, Fy, and Fz) and moment (Mx, My, Mz) on the most loaded BZ pin. Comparison, component by component, between SUB1 and GDM2 (left) and SUB2 and GDM2 (right).

4. Conclusions

In the present investigation, the possibility of extending the electromagnetic sub-modeling procedure, accomplished by transferring the boundary conditions from a primary (coarse) to a secondary (refined) mesh, well-proven for elements that have a magnetic-nodal formulation, was exploited for elements that have an edge-flux formulation that are much more performant than the former in non-linear analyses. The approach was demonstrated to be good enough to provide reliable EM inputs to be used as input for the structural analysis of the BB internal structure. Moreover, the performed study highlights the possibility of considering part of the excitation loads into the sub-models, allowing an increase in the element layers around the detailed region and reducing the error.

However, due to the edge formulation of SOLID236, the application of this methodology is limited to the case in which the boundary interface mesh (used to export/import the boundary DOFs) in the coarse and sub-model mesh is the same. An investigation of possible strategies to overcome this restriction is ongoing.

Author Contributions: Conceptualization, I.A.M., M.R. and F.L.; methodology, M.R.; software, M.R.; validation, M.R. and I.A.M.; formal analysis, M.R.; investigation, M.R. and I.A.M.; resources, I.A.M. and F.L.; data curation, I.A.M. and M.R.; writing—original draft preparation, I.A.M.; writing—review and editing, M.R. and F.L.; visualization, I.A.M. and M.R.; supervision, I.A.M. and F.L.; project administration, I.A.M.; funding acquisition, I.A.M. All authors have read and agreed to the published version of the manuscript.

Funding: This work was carried out within the framework of the EUROfusion Consortium, funded by the European Union via the Euratom Research and Training Programme (Grant Agreement No. 101052200–EUROfusion). Views and opinions expressed are, however, those of the author(s) only

and do not necessarily reflect those of the European Union or the European Commission. Neither the European Union nor the European Commission can be held responsible for them.

Data Availability Statement: Not applicable.

Conflicts of Interest: The authors declare no conflict of interest.

Abbreviations

The following abbreviations and acronyms are used in this manuscript:

DEMO	DEMOnstration power plant
ITER	International thermonuclear experimental reactor
BB	Breeding blanket
HCPB	Helium cooled pebble bed
FE	Finite element
EM	Electromagnetic
UVDE	Upper vertical displacement event
DOF	Degree of freedom
GDM1	Global DEMO model with coarse mesh
GDM2	Global DEMO model with detailed mesh in the sub-model region
SUB1	Sub-model with detailed mesh
SUB2	Extended sub-model(SUB1 + extended boundary layer of coarse mesh)
FW	First wall
BZ	Breeding zone
BSS	Back supporting structure
DOF	Degree of freedom
AZ	Magnetic edge-flux DOF
VOLT	Electric DOF
CURR	Plasma toroidal current
PSI_TOR	Plasma toroidal flux
R	Cylindrical radial coordinate
Z	Cylindrical vertical coordinate
PFV	Plasma poloidal field variation
TFV	Plasma toroidal field variation
PFC	Poloidal field coil
CS	Central solenoid
TFC	Toroidal field coil
B	Magnetic flux density
J	Electric current density
TQ	Thermal quench
CQ	Current quench

References

1. Turner, M.J.; Clough, R.W.; Martin, H.C.; Topp, L.J. Stiffness and deflection analysis of complex structures. *J. Aeronaut. Sci.* **1956**, *23*, 805–823. [CrossRef]
2. Hutton, D.V. *Fundamental of Finite Element Analysis*, 1st ed.; McGraw Hill Companies: New York, NY, USA, 2004.
3. Available online: https://www.iter.org/ (accessed on 25 January 2023).
4. Available online: https://www.euro-fusion.org/programme/demo/ (accessed on 25 January 2023).
5. Hirai, I.; Wang, B.P.; Pilkey, W.D. An efficient zooming method for finite element analysis. *Int. J. Numer. Methods Eng.* **1984**, *20*, 1671–1683. [CrossRef]
6. Hirai, I.; Uchiyama, Y.; Mizuta, Y.; Pilkey, W.D. An exact zooming method. *Finite Elem. Anal. Des.* **1985**, *1*, 61–69. [CrossRef]
7. Kondo, M.; Sinclair, G.B. A simple substructuring procedure for finite element analysis of stress concentrations. *Commun. Appl. Numer. Methods* **1985**, *1*, 215–218. [CrossRef]
8. Sun, C.T.; Mao, K.M. A global-local finite element method suitable for parallel computations. *Comput. Struct.* **1988**, *29*, 309–315. [CrossRef]
9. Marin, A.; Bertolini, C.; Lucca, F.; Ma, Y.; Pagani, I.; Vayakis, G.; Viganò, F.; Wälsh, M. ITER Magnetic sensor platform Engineering analyses. *Fusion Eng. Des.* **2019**, *146*, 2644–2648. [CrossRef]
10. Testoni, P.; Fanni, A.; Sonato, P. A sub-modeling approach for the electromechanical disruption analysis of the ITER ICH Antenna. *Fusion Eng. Des.* **2008**, *83*, 695–701. [CrossRef]

11. Khan, S.H.; Cai, M.; Grattan, K.T.V.; Kajan, K.; Honeywood, M.; Mills, S. Design and investigation of high-speed, large-force and long lifetime electromagnetic actuators by finite element modelling. *J. Phys. Conf. Ser.* **2005**, *15*, 300–305. [CrossRef]
12. Curreli, C.; Di Puccio, F.; Mattei, L. Application of the finite element submodeling technique in a single point contact and wear problem. *Int. J. Numer. Methods. Eng.* **2018**, *116*, 708–722. [CrossRef]
13. Cormier, N.G.; Smallwood, B.S.; Sinclair, G.B.; Meda, G. Aggressive submodelling of stress concentrations. *Int. J. Numer. Meth. Eng.* **1999**, *46*, 889–909. [CrossRef]
14. Aristovich, K.Y.; Khan, S.H. A new submodelling technique for multi-scale finite element computation of electromagnetic fields: Application in bioelectromagnetism. *J. Phys. Conf. Ser.* **2010**, *238*, 012050. [CrossRef]
15. Pina-Estany, J.; Colominas, C.; Fraxedas, J.; Llobet, J.; Perez-Murano, F.; Puigoriol-Forcada, J.M.; Ruso, D.; Garcia-Granada, A. A statistical analysis of nanocavities replication applied to injection moulding. *Int. Commun. Heat Mass Transf.* **2017**, *81*, 131–140. [CrossRef]
16. Kitamura, M.; Ohtsubo, H.; Akiyama, A.; Bandoh, H. Submodeling analysis of ship structure with superconvergent patch recovery method. *Int. J. Offshore Polar Eng.* **2003**, *13*, 216–222.
17. Mao, K.M.; Sun, C.T. A refined global-local finite element analysis method. *Int. J. Numer. Methods Eng.* **1991**, *32*, 29–43. [CrossRef]
18. Katagiri, H.; Semba, K.; Sano, H.; Mimura, N.; Yamada, T. Fast calculation of AC copper loss for high speed machines by zooming method. *IEEJ J. Ind. Appl.* **2017**, *6*, 395–400. [CrossRef]
19. Kowalski, M.; Kreischer, C. Metrological and numerical Validation of electromagnetic Sub-Model Techniques for 3D-FEM. In Proceedings of the 23rd International Conference on the Computation of Electromagnetic Fields, Cancun, Mexico, 16–20 January 2022.
20. Mergia, K.; Boukos, N. Structural, thermal, electrical and magnetic properties of Eurofer 97 steel. *J. Nucl. Mater.* **2008**, *373*, 1–8. [CrossRef]
21. DEMO1 Reference Design-2017 March ("EU DEMO1 2017")-PROCESS Two Page Output. Available online: http://idm.euro-fusion.org/?uid=2NE9JA&version=v1.0 (accessed on 25 January 2023).
22. Hernández, F.A.; Pereslavtsev, P.; Zhou, G.; Kang, Q.; D'Amico, S.; Neuberger, H.; Boccaccini, L.V.; Kiss, B.; Nádasi, G.; Maqueda, L.; et al. Consolidated design of the HCPB Breeding Blanket for the pre-Conceptual Design Phase of the EU DEMO and harmonization with the ITER HCPB TBM program. *Fusion Eng. Des.* **2020**, *157*, 111614. [CrossRef]
23. Villone, F. PMI-5.3.1-T006-D001-Report on 3D Disruption Studies and Vertical Stability Studies. Available online: https://idm.euro-fusion.org/default.aspx?uid=2MNKBE&version=v1.2 (accessed on 25 January 2023).
24. Maione, I.A.; Roccella, M.; Hernández, F.A.; Lucca, F. Update of electromagnetic loads on HCPB breeding blanket for DEMO 2017 configuration. *Fusion Eng. Des.* **2020**, *156*, 111604. [CrossRef]
25. ANSYS APDL Reference Manual. Available online: https://www.ansys.com/ (accessed on 25 January 2023).